A numerically accurate and robust expression for bistatic scattering from a plane triangular facet

Wendelboe, Gorm; Jacobsen, Finn; Bell, Judith

Published in:
Acoustical Society of America. Journal

Link to article, DOI:
10.1121/1.2149842

Publication date:
2006

Document Version
Publisher's PDF, also known as Version of record

Citation (APA):
Wendelboe, G., Jacobsen, F., & Bell, J. (2006). A numerically accurate and robust expression for bistatic scattering from a plane triangular facet. *Acoustical Society of America. Journal*, *119*(2), 701-704. https://doi.org/10.1121/1.2149842

LETTERS TO THE EDITOR

This Letters section is for publishing (a) brief acoustical research or applied acoustical reports, (b) comments on articles or letters previously published in this Journal, and (c) a reply by the article author to criticism by the Letter author in (b). Extensive reports should be submitted as articles, not in a letter series. Letters are peer-reviewed on the same basis as articles, but usually require less review time before acceptance. Letters cannot exceed four printed pages (approximately 3000–4000 words) including figures, tables, references, and a required abstract of about 100 words.

A numerically accurate and robust expression for bistatic scattering from a plane triangular facet (L)

Gorm Wendelboe[a)]

Danish Defense Research Establishment (DDRE), Ryvangs Allé 1, DK-2100 Copenhagen and Ørsted-DTU, Technical University of Denmark, Ørsteds Plads, Building 348, DK-2800 Kgs. Lyngby, Denmark

Finn Jacobsen[b)]

Ørsted-DTU, Technical University of Denmark, Ørsteds Plads, Building 348, DK-2800 Kgs. Lyngby, Denmark

Judith M. Bell[c)]

School of Engineering and Physical Sciences, Heriot-Watt University, Edinburgh, United Kingdom

(Received 18 March 2005; revised 22 July 2005; accepted 16 November 2005)

This work is related to modeling of synthetic sonar images of naval mines or other objects. Considered here is the computation of high frequency scattering from the surface of a rigid 3D-object numerically represented by plane triangular facets. The far field scattered pressure from each facet is found by application of the Kirchhoff approximation. Fawcett [J. Acoust. Soc. Am. **109**, 1319–1320 (2001)] derived a time domain expression for the backscattered pressure from a triangular facet, but the expression encountered numerical problems at certain angles, and therefore, the effective ensonified area was applied instead. The effective ensonified area solution is exact at normal incidence, but at other angles, where singularities also exist, the scattered pressure will be incorrect. This paper presents a frequency domain expression generalized to bistatic scattering written in terms of sinc functions; it is shown that the expression improves the computational accuracy without loss of robustness. © *2006 Acoustical Society of America.*

[DOI: 10.1121/1.2149842]

PACS number(s): 43.20.Fn, 43.20.Px [MO] Pages: 701–704

I. INTRODUCTION

In the past decade low price hardware has made high frequency sonar imagery systems widely available for naval-mine identification, harbor surveillance, and offshore industry. This work is related to the generation synthetic sonar images of naval mines and other objects.

An object will be numerically represented by elementary facets. The far field scattered pressure from each facet is found by application of the physical optics solution or Kirchhoff approximation.[1,2] The total scattered field is given as the coherent sum of pressure contributions from all nonshadowed facets.

The plane rectangular facet has been used by Sammelmann[3] and George.[4] However, for arbitrarily shaped objects the plane rectangular facet can lead to problems concerning correct surface representation. The plane triangular facet, on the other hand, is suited for all types of surfaces because of its co-planar property. Fawcett[5] derived the time domain impulse response for backscattering from a plane triangular facet. An alternative to the flat facet approach is the application of nonuniform rational B-spline surfaces (NURBS).[6] The field integral is evaluated over a parametric space of Bezier surfaces using the method of stationary phase.

The plane triangular facet is considered in this note. The expression for the scattered pressure from the plane triangular facet, first presented by Fawcett,[5] consists of three contributions corresponding to a response from each of the three vertices. However, this vertex response, which is applicable in the time domain, becomes numerically unstable at certain angles as the angle dependent coefficients get very large due to division by very small numbers. One way to deal with this is to replace the integral solution with the effective ensonified area, when the coefficients exceed, say, 1000.[5] This

a)Electronic mail: gw@oersted.dtu.dk
b)Electronic mail: fja@oersted.dtu.dk
c)Electronic mail: j.bell@hw.ac.uk

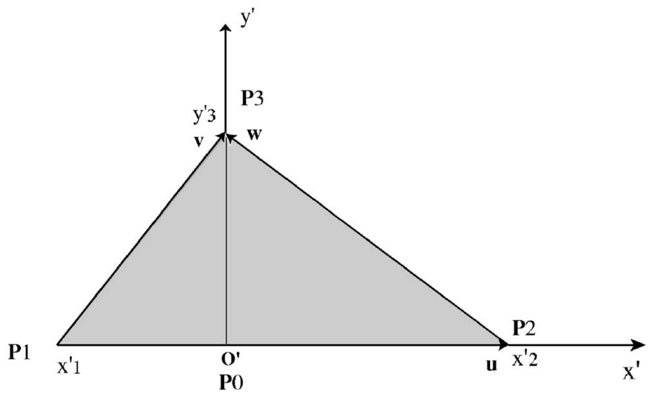

FIG. 1. Local coordinate system (′) of a plane triangular facet.

choice might be appropriate for near normal incidence, but for angles away from near normal incidence, where singularities also exist, the scattered pressure will be incorrect. In this note the time domain opportunity is abandoned and the frequency domain expression is rewritten in a numerically robust frame formulated additionally for bistatic scattering.

II. FACET-GEOMETRY AND FIELD APPROXIMATIONS

In this section a scattering integral for a rigid, plane and triangular facet is derived. The Kirchhoff approximation as well as the far field approximation are applied.

Suppose an arbitrarily shaped body is numerically represented by plane triangular facets. Each facet in the three-dimensional space is represented by its vertex points $\mathbf{P}_1$, $\mathbf{P}_2$, $\mathbf{P}_3$ and the unit surface normal vector, $\hat{\mathbf{n}}_s$, pointing out of the body. The vectors connecting the vertex points are defined by $\mathbf{u}=\overrightarrow{\mathbf{P}_1\mathbf{P}_2}$, $\mathbf{v}=\overrightarrow{\mathbf{P}_1\mathbf{P}_3}$, and $\mathbf{w}=\overrightarrow{\mathbf{P}_2\mathbf{P}_3}$, and they are arranged such that $\mathbf{u}$ represents the longest side of the triangle and $(\mathbf{u}\times\mathbf{v})\cdot\hat{\mathbf{n}}_s>0$; see Fig. 1.

A local coordinate system (′) is introduced. The origin $\mathbf{O}'$ has the global coordinates $\mathbf{P}_0=\mathbf{P}_1+\mathbf{v}_\mathbf{u}$, where $\mathbf{v}_\mathbf{u}$ is the projection of $\mathbf{v}$ on $\mathbf{u}$. In the local coordinate system the triangle is described by the axis-points x_1', x_2', and y_3'. The base of (′) is

$$\mathbf{e}_x'=\mathbf{u}/|\mathbf{u}|, \tag{1a}$$

$$\mathbf{e}_y'=(\mathbf{v}-\mathbf{v}_\mathbf{u})/|\mathbf{v}-\mathbf{v}_\mathbf{u}|, \tag{1b}$$

$$\mathbf{e}_z'=\mathbf{e}_x'\times\mathbf{e}_y'. \tag{1c}$$

The base given by Eqs. (1a)–(1c) establishes a coordinate transformation matrix applied on $\mathbf{r}_0$, the vector from $\mathbf{P}_0$ to the source, and on $\mathbf{r}_1$, the vector from $\mathbf{P}_0$ to the observation point. In the (′)-coordinate system $\mathbf{r}_0$ and $\mathbf{r}_1$ have been transformed into $\mathbf{r}_0'$ and $\mathbf{r}_1'$, respectively, but their (Euclidian) lengths are unchanged, i.e., $|\mathbf{r}_0'|=|\mathbf{r}_0|=r_0$ and $|\mathbf{r}_1'|=|\mathbf{r}_1|=r_1$. The unit surface normal vector has been transformed into $\hat{\mathbf{n}}_s'\equiv[001]^T$, and each point on the plane facet, S, is given by $\mathbf{x}_s'\equiv[x'y'0]^T$; see Fig. 2.

The Kirchhoff approximation is applied on the rigid surface and the total pressure field, p, is related to the incoming field, p_{inc}, through

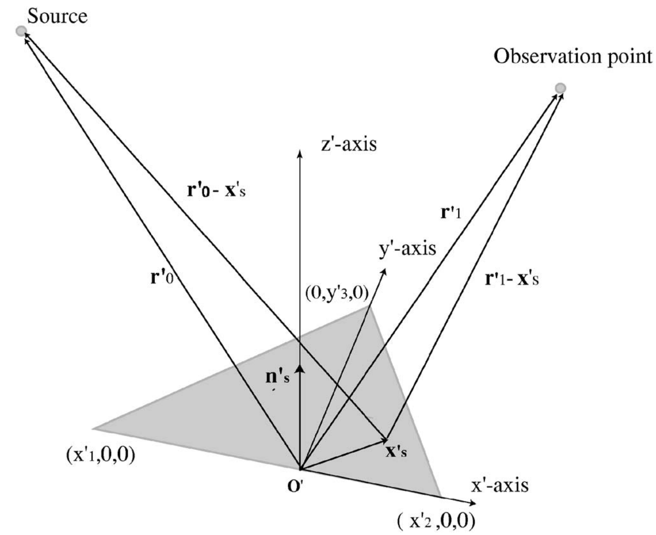

FIG. 2. Geometry applied for field integration over the surface of a triangular facet.

$$p(\mathbf{x}_s')=2p_{\text{inc}}(\mathbf{x}_s') \tag{2}$$

(see, e.g., Fawcett[5]). The Kirchhoff Helmholtz integral equation [see, e.g., Pierce,[7] Eq. (4-6.4)] consequently reduces to the integral

$$p_{\text{sc}}(\mathbf{r}_1')=\frac{1}{2\pi}\int_S p_{\text{inc}}(\mathbf{x}_s')\,\nabla G(\mathbf{x}_s'|\mathbf{r}_1')\cdot\hat{\mathbf{n}}_s'\,dS, \tag{3}$$

where $p_{\text{sc}}(\mathbf{r}_1')$ is the facet-scattered pressure measured at the observation point, $\mathbf{r}_1'$, and $\nabla G(\mathbf{r}_1'|\mathbf{x}_s')$ is the gradient of the free space Green's function directed toward the observation point. The incoming field originates from a monopole source,

$$p_{\text{inc}}(\mathbf{x}_s')=p_0\frac{e^{ik|\mathbf{x}_s'-\mathbf{r}_0'|}}{|\mathbf{x}_s'-\mathbf{r}_0'|}, \tag{4}$$

where p_0 is the pressure amplitude 1 meter from the source. In the far field, the range from the facet to the source by far exceeds the dimensions of the facet, and hence, a first order Taylor series expansion of $|\mathbf{x}_s'-\mathbf{r}_0'|$ with respect to $\mathbf{x}_s'/r_0$ is possible,

$$|\mathbf{x}_s'-\mathbf{r}_0'|\approx r_0-\hat{\mathbf{r}}_0'\cdot\mathbf{x}_s', \tag{5}$$

where $\hat{\mathbf{r}}_0'=\mathbf{r}_0'/r_0$ [see, e.g., Ogilvy,[1] Eq. (4.10)]. The right-hand side of Eq. (5) will be applied for the phase term of Eq. (4) whereas it is sufficient to approximate the slowly varying denominator in Eq. (4), i.e., the term that represents geometrical spreading, to zero order, that is, $|\mathbf{x}_s'-\mathbf{r}_0'|\approx r_0'$. The incoming field is

$$p_{\text{inc}}(\mathbf{x}_s')=p_0\frac{e^{ikr_0}}{r_0}e^{-ik\hat{\mathbf{r}}_0'\cdot\mathbf{x}_s'}, \tag{6}$$

and hence, the part of the spherical wave that sweeps over the facet is considered locally plane. The gradient of the Green's function,

$$\nabla G(\mathbf{r}'_1|\mathbf{x}'_s) = \frac{\mathbf{r}'_1 - \mathbf{x}'_s}{|\mathbf{r}'_1 - \mathbf{x}_s|^3}(ik|\mathbf{r}'_1 - \mathbf{x}_s| - 1)e^{ik|\mathbf{r}'_1 - \mathbf{x}'_s|}, \quad (7)$$

[see, e.g., Pierce,[7] Eq. (4-6.5)] is also approximated to the far field. In the phase term, $|\mathbf{r}'_1 - \mathbf{x}'_s| \approx r_1 - \hat{\mathbf{r}}'_1 \cdot \mathbf{x}'_s$, is applied, and in the amplitude terms, $\mathbf{r}'_1 - \mathbf{x}'_s \approx \mathbf{r}'_1$ is used. The expression within the brackets of Eq. (7) is approximated to $(ik|\mathbf{r}'_1 - \mathbf{x}'_s| - 1) \approx (ikr_1 - 1) \approx ikr_1$, where the second approximation is valid because $ikr_1 \gg 1$. Hence,

$$\nabla G(\mathbf{r}'_1|\mathbf{x}'_s) = \hat{\mathbf{r}}'_1 ik \frac{e^{ikr_1}}{r_1} e^{-ik\hat{\mathbf{r}}'_1 \cdot \mathbf{x}'_s}, \quad (8)$$

where $\hat{\mathbf{r}}'_1 = \mathbf{r}'_1 / r_1$. Insertion of Eq. (6) and Eq. (7) into Eq. (3) leads to a scattering integral with a linear phase term

$$p_{\mathrm{sc}}(\mathbf{x}) = \frac{p_0 ike^{ik(r_0+r_1)}\hat{\mathbf{r}}'_1 \cdot \hat{\mathbf{n}}'_s}{2\pi r_0 r_1} \int_S e^{-ik(\hat{\mathbf{r}}'_0 + \hat{\mathbf{r}}'_1)\cdot \mathbf{x}'_s} \, dS. \quad (9)$$

III. A ROBUST EXPRESSION FOR TRIANGULAR FACET SCATTERING

If the phase variation over the facet is neglected, the integral in Eq. (9) can be replaced by the facet area, S, and the approximate effective ensonified area response is

$$p_{\mathrm{sc}}(\mathbf{x}) = \frac{p_0 ike^{ik(r_0+r_1)} \cos \theta_1}{2\pi r_0 r_1} S, \quad (10)$$

where $\cos \theta_1 = \hat{\mathbf{r}}'_1 \cdot \hat{\mathbf{n}}'_s$. However, this expression is only exact for normal incidence. In the general case the dot-product in the exponential term of the surface integral Eq. (9) must be considered,

$$(\hat{\mathbf{r}}'_0 + \hat{\mathbf{r}}'_1) \cdot \mathbf{x}'_s = ax' + by', \quad (11)$$

where the angle dependent constants are given by

$$a = \sin \theta_0 \cos \varphi_0 + \sin \theta_1 \cos \varphi_1, \quad (12a)$$

$$b = \sin \theta_0 \sin \varphi_0 + \sin \theta_1 \sin \varphi_1, \quad (12b)$$

and where the angle between $\mathbf{r}'_j$ and $\mathbf{n}'_s$ is $0 \le \theta_j \le \pi/2$, and the angle in the $x'y'$ plane is $0 \le \varphi_j \le 2\pi$, $j = 0, 1$. The solution to Eq. (9) is brought on the vertex response form

$$p_{\mathrm{sc}}(\mathbf{x}) = \frac{p_0 e^{ik(r_0+r_1)} \cos \theta_1}{ik2\pi r_0 r_1}[\kappa_1 e^{-ikax'_1} + \kappa_2 e^{-ikax'_2} + \kappa_3 e^{-ikby'_3}], \quad (13a)$$

where κ_1, κ_1, and κ_3 are the vertex coefficients given by

$$\kappa_1 = \frac{-y'_3}{a(ax'_1 - by'_3)}, \quad (13b)$$

$$\kappa_2 = \frac{y'_3}{a(ax'_2 - by'_3)}, \quad (13c)$$

$$\kappa_3 = \frac{y'_3(x'_2 - x'_1)}{(ax'_2 - by'_3)(ax'_1 - by'_3)}. \quad (13d)$$

The vertex response can be transformed into the time domain to obtain the impulse response (see, e.g., Fawcett[5]). As can be observed from Eqs. (13b)–(13d) three singularities are present, $a=0$, $ax'_1 - by'_3 = 0$, and $ax'_2 - by'_3 = 0$. For backscattering these singularities correspond to incident directions normal to the three sides of the triangle, i.e., normal to $\mathbf{u}$, $\mathbf{w}$ or $\mathbf{v}$. From an analytical point of view, large values of κ_j will cancel each other in Eq. (13a). However, in a numerical implementation the cancellation tends to fail because of truncation errors obtained near the working precision of the computer. In what follows the time domain approach is abandoned and a numerically robust expression is derived. The angle dependent terms a, $(ax'_1 - by'_3)$, and $(ax'_2 - by'_3)$ are separated and expressed in terms of the well-behaved sinc function. Hence, the solution to Eq. (9) is written

$$\begin{aligned} p_{\mathrm{sc}}(\mathbf{x}) = {} & \frac{p_0 e^{ik(r_0+r_1)} \cos \theta_1}{2\pi r_0 r_1}\left(\frac{1}{ikb}\right) \\ & \times \left[x'_1 e^{-ik(ax'_1 + by'_3)/2} \frac{\sin(k[ax'_1 - by'_3]/2)}{k[ax'_1 - by'_3]/2} \right. \\ & - x'_2 e^{-ik(ax'_2 + by'_3)/2} \frac{\sin(k[ax'_2 - by'_3]/2)}{k[ax'_2 - by'_3]/2} \\ & \left. + (x'_2 - x'_1) e^{-ika(x'_1 + x'_2)/2} \frac{\sin(ka[x'_2 - x'_1]/2)}{ka[x'_2 - x'_1]/2} \right]. \end{aligned} \quad (14a)$$

When $b \to 0$, Eq. (14a) becomes numerically unstable, and is replaced by the limit value, $p_{\mathrm{sc}}(\mathbf{x})$ for $b \to 0$, found by using the rule of L'Hospital,

$$\begin{aligned} p_{\mathrm{sc}}(\mathbf{x}) = {} & \frac{p_0 e^{ik(r_0+r_1)} \cos \theta_1 y'_3}{4\pi i r_0 r_1} \times [g(kax'_1/2)x'_1 e^{-ikax'_1/2} \\ & - g(kax'_2/2)x'_2 e^{-ikax'_2/2}], \end{aligned} \quad (14b)$$

where

$$g(x) = \frac{-\cos(x) + \sin(x)/x}{x} - i\frac{\sin(x)}{x}. \quad (14c)$$

IV. RESULTS

Validation is carried out by considering the canonical problem of backscattering of a plane wave of unit amplitude from a rigid sphere. The infinite harmonic series solution[8] is the Benchmark solution. The sphere is a good test case because sharp edges, where the Kirchhoff approximation fails, are absent. The time domain response of a 445 kHz Ricker pulse incident on a sphere with a radius equal to 10 centimeters measured at a range of 10 meters is determined. In the numerical model the surface of the sphere is represented by iso-sized facets with areas of 11 mm^2. Results from three different numerical Kirchhoff approaches are considered. The first approach is the vertex response given by Eqs. (13) where no numerical precautions are taken. In the second approach the vertex response is combined with the effective area response given by Eq. (10) according to Fawcett.[5] The vertex response is switched "off" and the effective area response "on" when the magnitude of one of the coefficients in Eqs. (13) exceed 1000. Finally, the third ap-

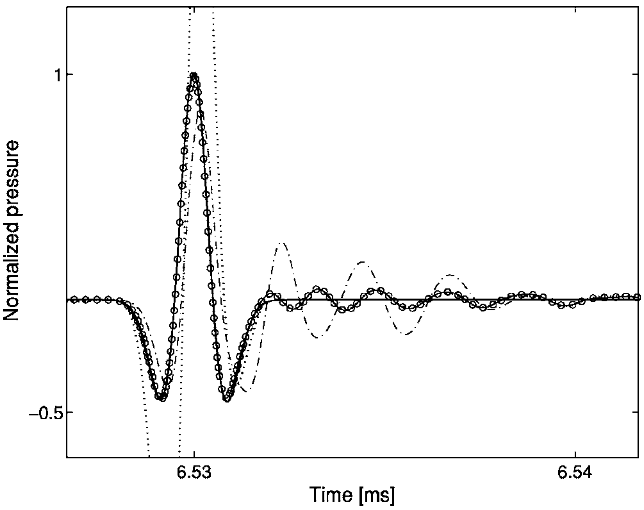

FIG. 3. Backscattering from a rigid sphere. The thick solid line is the benchmark solution; the dotted line is the vertex response [Eq. (13)] the dashed-dotted line is the vertex response, [Eq. (13)], combined with the effective area response [Eq. (10)]; and the solid line with circles is the robust response [Eq. (14)].

proach is the robust response given by Eq. (14). Fourier synthesis has been carried out on the benchmark solution as well as on the three different numerical Kirchhoff approaches.

The results are given in Fig. 3. The robust response given by Eq. (14) matches the analytic solution very well except after the specular reflection where oscillations occur. These oscillations are related to the numerical surface discretization of the sphere and not the scattering formulas. The result from the pure vertex response, Eqs. (13), clearly diverges from the analytical solution at the specular reflection, but after that, it quickly approaches the robust response. Hence, the pure vertex response is accurate as long as the critical angles are not encountered; if this happens, erroneous results orders of magnitudes from the actual response will occur. The combined solution is significantly closer to the analytical result at the specular reflection, but exhibits stronger oscillations after the specular reflection, indicating that the combined approach is a robust, but not very accurate, numerical approach when singularities are encountered. The robust response expressed in terms of sinc functions has proven to be the most numerically reliable expression.

V. CONCLUSION

A numerically robust expression for the far field bistatic scattered pressure from a plane triangular facet written in terms of sinc functions, Eq. (14), has been presented. The expression is applied for the computation of high frequency scattering from arbitrarily shaped objects. Equation (14) has been compared with two solutions based on the vertex response expression, Eq. (13). The first solution is the pure vertex response which is numerically unstable at certain angles. The second solution, presented by Fawcett,[5] combines Eq. (13) with the effective ensonified area, Eq. (10), in the case where one of the coefficients of the vertex response, Eqs. (13b)–(13d), exceeds a threshold value equal to 1000. Comparisons have been carried out by considering the canonical problem of backscattering of a plane wave from a rigid sphere, and the expression written in terms of sinc functions has been shown to be the most reliable solution in terms of accuracy.

ACKNOWLEDGMENT

The authors gratefully acknowledge communication with John Fawcett at DRDC, Atlantic.

[1]J. A. Ogilvy, *Theory of Wave Scattering from Random Rough Surfaces* (IOP, London, 1991), Chap. 4.1.

[2]H. Medwin and C. S. Clay, *Fundamentals of Acoustical Oceanography* (Academic Press, London, 1998), Chap. 7.2.3.

[3]G. S. Sammelman, "Propagation and scattering in very shallow water," Proc. IEEE Oceans **1**, 337–344 (2001).

[4]O. George and R. Bahl, "Simulation of backscattering of high frequency sound from complex objects and sand sea-bottom," IEEE J. Ocean. Eng. **20**, 119–130 (1995).

[5]J. A. Fawcett, "Modeling of high-frequency scattering from objects using a hybrid Kirchhoff/diffraction approach," J. Acoust. Soc. Am. **109**, 1312–1319 (2001).

[6]J. Perez and M. F. Catedra, "Application of physical optics to the RCS computation of bodies modeled with NURBS surfaces," IEEE Trans. Antennas Propag. **42**, 1404–1411 (1994).

[7]A. D. Pierce, *Acoustics. An Introduction to its Physical Principles and Applications* (Acoustical Society of America, New York, 1991), second printing.

[8]E. G. Williams, *Fourier Acoustics. Sound Radiation and Nearfield Acoustical Holography* (Academic Press, London, 1999), Eq. (6.185).